RSC Advances

PAPER

Cite this: *RSC Adv.*, 2015, **5**, 90720

Achieving visible light excitation in carbazole-based Eu^{3+}–β-diketonate complexes *via* molecular engineering†

Biju Francis,[ab] Christian Heering,[b] Ricardo O. Freire,[c] M. L. P. Reddy*[a] and Christoph Janiak*[b]

Received 14th September 2015
Accepted 13th October 2015

DOI: 10.1039/c5ra18819a

www.rsc.org/advances

Herein, we present the synthesis, characterization and photophysical properties of a series of Eu^{3+} complexes prepared with novel carbazole-based fluorinated β-diketones, namely, 4,4,5,5,5-pentafluoro-3-hydroxy-1-(9-phenyl-9*H*-carbazol-2-yl)pent-2-en-1-one (**L1**) and 4,4,5,5,5-pentafluoro-3-hydroxy-1-(9-(4-methoxyphenyl)-9*H*-carbazol-2-yl)pent-2-en-1-one (**L2**) as primary ligands and a bidentate phosphine oxide molecule, 4,5-bis(diphenylphosphino)-9,9-dimethylxanthene oxide (DDXPO) as ancillary ligand. Using the Sparkle/PM3 model the molecular geometries of the designed complexes are optimized and the luminescent parameters are calculated by the LUMPAC software. The results demonstrated that suitably expanded π-conjugation in the developed Eu^{3+}–carbazole based β-diketonate complexes dramatically red-shifted the excitation maximum to the visible region ($\lambda_{ex,max}$ = 420 nm) with an impressive quantum yield (34–42%). The triplet state energy levels of **L1** and **L2** in the complexes are higher than that of the lowest excited level of Eu^{3+} ion, $^5D_0$, so the photoluminescence mechanism of the Eu^{3+} complexes was proposed as a ligand-sensitized luminescence process. The predicted luminescent parameters from the Sparkle/PM3 structures are in agreement with the experimental data, which shows the efficacy of the theoretical models adopted in the present study.

Introduction

Capitalizing on the unique and appealing spectroscopic characteristics of Eu^{3+} ions, its complexes have been utilized for a myriad of applications in domains as diverse as biomedical analysis (fluoroimmunoassays, FRET microscopy and cellular imaging),[1–5] sensing (pH, temperature, pathogens and toxic gases/ions)[6–11] and materials science (organic light emitting diodes and solar cells).[12–19] The advantageous features of Eu^{3+} ions include long excited-state lifetimes (μs to ms range) and narrow, easily recognizable line-like emission bands with large Stokes shifts.[20–24] The major obstacle in adopting Eu^{3+} for relevant applications arises due to its weak absorbance (molar absorption coefficients less than 10 L mol^{-1} cm^{-1}) because of the parity forbidden intra 4f–4f transitions.[25–27] Fortunately, this handicap is easily overcome by coordinating Eu^{3+} ions to suitable organic ligands which upon irradiation, absorb energy and transfer this energy to the metal center by the "antenna effect".[28–31] Carbazole-based ligands are widely acknowledged for their role as antenna molecules for the Eu^{3+} ion by virtue of their modest cost, excellent hole transporting properties, easily tunable opto-electronic properties and their high chemical and environmental stabilities.[32–34]

There is a rapidly increasing demand for less-harmful biomarkers in life sciences and low-voltage-driven emitters in optoelectronics.[35–37] Owing to this scenario, the development of visible light excitable europium complexes has received great attention in the past decade.[38–43] Visible light is less harmful to biological tissues, allowing deep penetration, causing less background fluorescence and, thus, minimizing the interferences from biological samples.[44,45] Gong and co-workers reported visible

[a]*CSIR-Network of Institutes for Solar Energy, National Institute for Interdisciplinary Science & Technology (NIIST), Thiruvananthapuram-695 019, India. E-mail: mlpreddy55@gmail.com*

[b]*Universität Düsseldorf, Institut für Anorganische Chemie 1, Universitätsstr. 1, 40225 Düsseldorf, Germany. E-mail: janiak@uni-duesseldorf.de*

[c]*Pople Computational Chemistry Laboratory, Universidade Federal de Sergipe, 49100-000, Sao Cristovaáo, Sergipe, Brazil*

† Electronic supplementary information (ESI) available: ^1H NMR spectrum of ligand **L2**, FAB-MS spectra of complexes **1–6**, ^{31}P NMR spectrum of complex **4**, thermogravimetric curves for complexes **1**, **2** and **5**, overlay of crystal structure and Sparkle/PM3 model optimized structure of complex **A**, the ground state geometries of complexes **1**, **2**, **5** and **6** calculated using the Sparkle/PM3 model, UV-visible absorption spectra of the ligands **L1** and DDXPO and complexes **1**, **2** and **5** in $CHCl_3$ solution, solid state room temperature excitation (λ_{em} = 612 nm) and emission spectra (λ_{ex} = 400 nm) of complexes **1–4**, solid state luminescence decay profiles of complexes **1** and **2** monitored at 612 nm, 77 K phosphorescence spectra of complexes $Gd(\mathbf{L1})_3(C_2H_5OH)_2$ (**5**) and $Gd(\mathbf{L2})_3(C_2H_5OH)_2$ (**6**), comparison of selected bond lengths (Å) from crystal structure and Sparkle/PM3 model geometry for complex **A**, selected bond lengths (Å) for complexes **1–4** by Sparkle/PM3 model, selected bond angles (°) for complexes **1–4** by Sparkle/PM3 model, selected bond lengths (Å) for complexes **5** and **6** by Sparkle/PM3 model, selected bond angles (°) for complexes **5** and **6** by Sparkle/PM3 model. See DOI: 10.1039/c5ra18819a

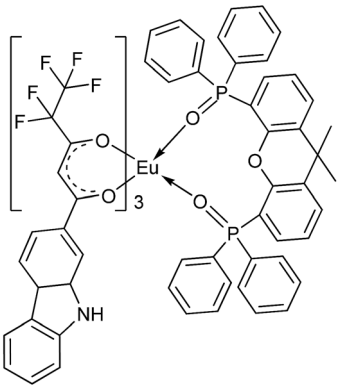

Fig. 1 Complex $Eu(CPFHP)_3(DDXPO)$[48] (**A**).

light excitable Eu^{3+} complexes using carbazole-based ligands by substituting the hydrogen atom on nitrogen with alkyl groups.[46] Also by introducing a $-CF_3$ group in the carbazole skeleton, they improved the luminescence quantum yield of the Eu^{3+} complexes to 34%.[47] Recently, our group reported a highly luminescent Eu^{3+} complex, $Eu(CPFHP)_3(DDXPO)$, (henceforth, referred to as complex **A**) using a carbazole-based fluorinated β-diketonate as the primary ligands and a phosphine oxide molecule as the neutral donor (Fig. 1).[48] However, the excitation window of the reported complex was in the UV region ($\lambda_{max} = 390$ nm), which limited its use in biological applications.

Along the lines of the foregoing results, we have, in the present study, tuned the physical properties of carbazole-based fluorinated β-diketonate complexes into promising candidates for biological applications by extending the π-conjugation of the ligand, thus, decreasing the band gap of the complexes and consequently shifting the excitation wavelength to the lower energy visible region. A series of new Eu^{3+} antenna complexes, which contain highly conjugated carbazole-based β-diketonates, **L1** (Scheme 1) and **L2** (Scheme 1) were synthesized. Here, 4,5-bis(diphenylphosphino)-9,9-dimethylxanthene oxide (DDXPO) has been chosen as the ancillary ligand. The newly synthesized Eu^{3+} complexes are characterized using various spectroscopic methods and their photophysical properties are investigated. From the photoluminescence studies we confirm that extension of π-conjugation in the organic ligand shifts the excitation window of the corresponding Eu^{3+} complexes towards the visible region. Also by introducing an electron donating $-OCH_3$ group, we improve the overall luminescence quantum yield and the luminescence lifetime values of Eu^{3+} complexes to 42% and 828 μs respectively, from 28% and 702 μs in the reference complex **A**. The molecular geometries of the designed complexes are optimized by the Sparkle/PM3 model and their spectroscopic parameters are theoretically calculated using the LUMPAC software.[49] Theoretical calculations of the photophysical properties of the complexes are in good agreement with the experimental values.

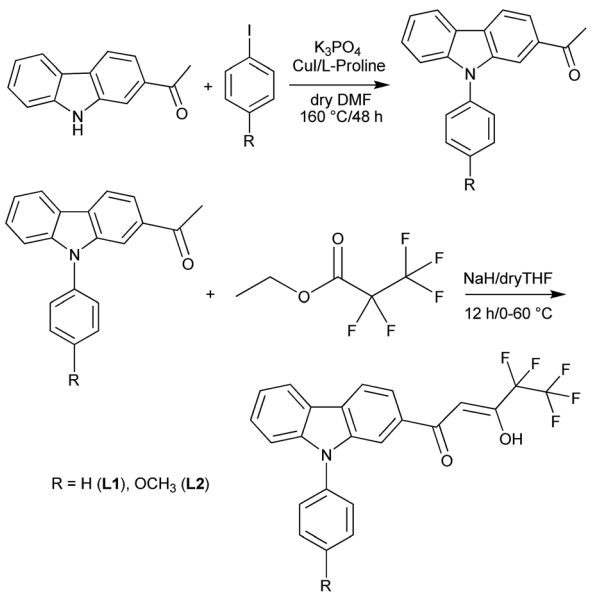

Scheme 1 Synthesis of ligands **L1** and **L2**.

Experimental

Materials and instrumentation

Europium(III) nitrate pentahydrate (99.9% purity), gadolinium(III) nitrate hexahydrate (99.9% purity), 2-acetylcarbazole (98% purity), iodobenzene (98% purity), 4-iodoanisole (98% purity), copper(I) iodide, potassium phosphate tribasic (98% purity), ethylpentafluoropropionate (98% purity) and sodium hydride (60% dispersion in mineral oil) were procured from Sigma-Aldrich. L-Proline (99% purity) was purchased from Alfa-Aesar. All the other chemicals used were of analytical reagent grade and were used without subsequent purification. Solvents were dried using standard methods. The bidentate phosphine oxide, 4,5-bis(diphenylphosphino)-9,9-dimethylxanthene oxide (DDXPO), was synthesized according to the method described in our earlier publication.[50]

Perkin-Elmer Series 2 Elemental Analyser 2400 was used to record the C, H, and N elemental analyses. The FT-IR spectra were taken using KBr pellets on a Perkin-Elmer Spectrum One FT-IR spectrometer operating between 4000 and 450 cm^{-1}. The ^1H NMR (500 MHz), ^{13}C NMR (125.7 MHz) and ^{31}P NMR (202.44 MHz) spectra of the new compounds were recorded in chloroform-d solution using a Bruker 500 MHz NMR spectrometer. The chemical shifts are reported in parts per million relative to tetramethylsilane ($SiMe_4$) for ^1H NMR and ^{13}C NMR spectra. The mass spectra were recorded using a JEOL JSM 600 fast atom bombardment (FAB) high resolution mass spectrometer (FAB-MS), and a TG/DTA-6200 instrument (SII Nano Technology Inc., Japan) was used to perform the thermogravimetric analyses. UV-visible absorption spectra were recorded with a Shimadzu, UV-2450 UV-vis spectrophotometer. All spectra were corrected for the background spectrum of the solvent. The absorbances of the ligands and complexes were measured in $CHCl_3$ solution. The solid state absorption spectra were recorded using UV-3600 UV-vis spectrophotometer, with $BaSO_4$ as reference. The PL spectra were recorded on a Spex-Fluorolog FL22 spectrofluorimeter equipped with a double grating 0.22 m Spex 1680 monochromator and a 450 W Xe lamp as the excitation source operating in the front face mode. The

lifetime measurements were carried out at room temperature using a Spex 1040 D phosphorimeter. The overall quantum yields for the Eu^{3+} complexes were determined under ligand excitation (390–420 nm) and are based on the absolute method using a calibrated integrating sphere in a Spex-Fluorolog spectrofluorimeter.[51] Xe-arc lamp was used to excite the samples placed in the sphere. The quantum yields were determined by comparing the spectral intensities of the lamp and the sample emission as reported in the literature.[52–54] Using this experimental setup and the integrating sphere system, the solid-state fluorescence quantum yield of tris-8-hydroxyquinolinolato aluminum (Alq_3) was determined to be 40%, which is consistent with previously reported values.[55,56] Each sample was measured several times under slightly different experimental conditions. The estimated error for the quantum yields is (±10%).[57]

Synthesis of the ligands

The ligands 4,4,5,5,5-pentafluoro-3-hydroxy-1-(9-phenyl-9*H*-carbazol-2-yl)pent-2-en-1-one (**L1**) and 4,4,5,5,5-pentafluoro-3-hydroxy-1-(9-(4-methoxyphenyl)-9*H*-carbazol-2-yl)pent-2-en-1-one (**L2**) were synthesized according to the route presented in Scheme 1.

Synthesis of 1-(9-phenyl-9*H*-carbazol-2-yl)ethanone

As shown in Scheme 1, the synthesis of 1-(9-phenyl-9*H*-carbazol-2-yl)ethanone was achieved by a typical substitution reaction. 2-Acetylcarbazole (2.3 mmol) was added to a round bottom flask containing 20 mL of anhydrous DMF. To this, K_3PO_4 (5 mmol) was added as base. 20 mol% of CuI and L-proline were added to the reaction mixture which act as catalyst and promoter respectively. The reaction mixture was refluxed for 48 h after the addition of 4-iodobenzene (2.3 mmol) at 160 °C. This was then allowed to cool to room temperature and poured into ice-cold water. The precipitate obtained was washed well with water, dried and purified by column chromatography (5% (v/v) ethyl acetate in hexane) to give the product as a yellowish solid (yield 75%). ^{1}H NMR (500 MHz, $CDCl_3$): δ (ppm) 8.17 (s, 2H), 8.02 (s, 1H), 7.91–7.89 (m, 1H), 7.63 (t, 2H, $J = 7.5$), 7.55 (d, 2H, $J = 10$), 7.52–7.25 (m, 4H), 2.66 (s, 3H). ^{13}C NMR (125 MHz, $CDCl_3$): δ (ppm) 197.3, 145.8, 137.1, 136.6, 134.5, 129.6, 127.1, 125.8, 121.7, 120.9, 120.1, 114.8, 111.5, 110.3, 109.8, 26.9. FAB-MS m/z = 286.34 (M^+ + H).

Synthesis of 4,4,5,5,5-pentafluoro-3-hydroxy-1-(9-phenyl-9*H*-carbazol-2-yl)pent-2-en-1-one (L1)

The ligand **L1** was synthesized by a modified Claisen condensation procedure. 1-(9-Phenyl-9*H*-carbazol-2-yl)ethanone (1 mmol) was dissolved in 20 mL of dry THF. To this, sodium hydride (2.5 mmol) was added under inert atmosphere at 0 °C and stirred for 1 h. After the reaction mixture turned orange-red, ethyl pentafluoropropionate (1.2 mmol) was added drop wise and the reaction mixture was then allowed to stir under inert atmosphere for 12 h. The reaction was then quenched with cold water, 2 M HCl (20 mL) was added, and the solution was extracted with dichloromethane (3 × 20 mL). The organic layer was dried over anhydrous Na_2SO_4, filtered and the solvent was evaporated. The product was then purified by column chromatography (5% (v/v) ethyl acetate in hexane) to give the product as yellowish crystals (yield 70%). Elemental analysis (%): calcd for $C_{23}H_{14}F_5NO_2$ (431.36): C, 64.04; H, 3.27; N, 3.25. Found: C, 64.24; H, 3.29; N, 3.30. ^{1}H NMR (500 MHz, $CDCl_3$): δ (ppm) 15.625 (broad, enol –OH), 8.24–8.19 (m, 2H), 8.03 (s, 1H), 7.85 (d, 1H, $J = 10$), 7.67 (t, 2H, $J = 7.5$), 7.57–7.49 (m, 4H), 7.42 (d, 1H, $J = 10$), 7.35 (t, 1H, $J = 7$), 6.70 (s, 1H). ^{13}C NMR (125 MHz, $CDCl_3$): δ (ppm) 198.2, 186.8, 158.3, 142.8, 140.8, 136.8, 130.3, 130.0, 128.3, 128.1, 127.3, 122.3, 121.3, 120.8, 120.6, 119.3, 110.4, 109.8, 94.7. FT-IR (KBr) ν_{max}: 3070, 1620, 1597, 1504, 1234 cm^{-1}. FAB-MS $m/z = 432.66$ (M^+ + H).

Synthesis of 1-(9-(4-methoxyphenyl)-9*H*-carbazol-2-yl) ethanone

A typical substitution reaction was used for the synthesis of 1-(9-(4-methoxyphenyl)-9*H*-carbazol-2-yl)ethanone. 2-Acetylcarbazole (2.3 mmol) was added to a round bottom flask containing 20 mL of anhydrous DMF. To this K_3PO_4 (5 mmol) was added as base. 20 mol% of CuI and L-proline were added to the reaction mixture which act as catalyst and promoter respectively. The reaction mixture was refluxed for 48 h after the addition of 4-iodoanisole (2.3 mmol) at 160 °C. The resultant reaction mixture was then allowed to cool to room temperature and poured into ice-cold water. The precipitate obtained was washed well with water, dried and purified by column chromatography (5% (v/v) ethyl acetate in hexane) to give the product as a yellowish solid (yield 73%). ^{1}H NMR (500 MHz, $CDCl_3$): δ (ppm) 8.18 (d, 2H, $J = 10$), 7.94 (s, 1H), 7.89 (d, 1H, $J = 10$), 7.48–7.43 (m, 3H), 7.35–7.29 (m, 2H), 7.14 (d, 2H, $J = 7$), 3.94 (s, 3H), 2.67 (s, 3H). ^{13}C NMR (125 MHz, $CDCl_3$): δ (ppm) 198.4, 159.2, 143.0, 141.1, 134.8, 129.6, 128.7, 127.4, 127.0, 122.2, 121.11, 120.2, 120.2, 120.0, 115.3, 110.1, 110.0, 55.7, 27.0. FAB-MS $m/z = 316.05$.

Synthesis of 4,4,5,5,5-pentafluoro-3-hydroxy-1-(9-(4-methoxyphenyl)-9*H*-carbazol-2-yl)pent-2-en-1-one (L2)

The ligand **L2** was synthesized by a modified Claisen condensation procedure. 1-(9-(4-Methoxyphenyl)-9*H*-carbazol-2-yl) ethanone (1 mmol) was dissolved in 20 mL of dry THF. To this, sodium hydride (2.5 mmol) was added under inert atmosphere at 0 °C and stirred for 1 h. After the reaction mixture turned orange-red, ethyl pentafluoropropionate (1.2 mmol) was added drop wise and the reaction mixture was allowed to stir under inert atmosphere for 12 h. The reaction was then quenched with water, 2 M HCl (20 mL) was added, and the solution was extracted with dichloromethane (3 × 20 mL). The organic layer was dried over anhydrous Na_2SO_4, filtered and the solvent was evaporated. The product was then purified by column chromatography (5% (v/v) ethyl acetate in hexane) to give the product as yellowish crystals (yield 70%). Elemental analysis (%): calcd for $C_{24}H_{16}F_5NO_3$ (461.38): C, 62.48; H, 3.50; N, 3.04. Found: C, 62.64; H, 3.59; N, 3.10. ^{1}H NMR (500 MHz, $CDCl_3$, see Fig. S1 in ESI†): δ (ppm) 15.77 (broad, enol –OH), 8.23–8.19 (m, 2H), 7.95 (s, 1H), 7.84 (d, 1H, $J = 10$), 7.50 (t, 1H, J

= 7.5), 7.45 (d, 2H, J = 10), 7.36–7.32 (m, 2H), 7.16 (d, 2H, J = 10), 6.71 (s, 1H), 3.95 (s, 3H). ^{13}C NMR (125 MHz, $CDCl_3$): δ (ppm) 198.4, 186.9, 159.4, 143.2, 141.1, 129.9, 129.2, 128.6, 128.1, 128.0, 122.2, 121.1, 120.2, 120.1, 120.0, 115.3, 110.3, 109.7, 93.8, 55.6. FT-IR (KBr) ν_{max}: 2949, 2837, 1618, 1595, 1520, 1233 cm^{-1}. FAB-MS m/z = 462.36 (M^+ + H).

Synthesis of solvated lanthanide β-diketonate complexes

A mixture of the relevant β-diketonate ligand, **L1** or **L2**, (0.6 mmol) and NaOH (0.6 mmol) in 10 mL ethanol was stirred at room temperature for 10 min, following which a saturated ethanolic solution of $Ln(NO_3)_3 \cdot nH_2O$ (0.2 mmol) was added drop wise, and the reaction mixture stirred subsequently for 24 h (Scheme 2). 20 mL water was then added, and the precipitate formed was filtered off, washed again with water (3 × 10 mL), dried and purified by recrystallization from THF–water (10 : 90) mixture.

Eu(**L1**)$_3$(C_2H_5OH)$_2$ (**1**). Elemental analysis (%): calcd for $C_{73}H_{51}F_{15}N_3O_8Eu$ (1535.26): C, 57.11; H, 3.35; N, 2.74. Found: C, 57.23; H, 3.39; N, 2.75. FT-IR (KBr) ν_{max}: 3440 (b), 2957, 2934, 1607, 1514, 1234 cm^{-1}. FAB-MS m/z = 1443.36 ($M^+ - 2C_2H_5OH$), 1013.32 (M^+ − **L1** − $2C_2H_5OH$), 582.84 ($M^+ - 2$**L1** − $2C_2H_5OH$) (Fig. S2 in ESI†).

Gd(**L1**)$_3$(C_2H_5OH)$_2$ (**5**). Elemental analysis (%): calcd for $C_{73}H_{51}F_{15}N_3O_8Gd$ (1540.43): C, 56.92; H, 3.34; N, 2.73. Found: C, 57.03; H, 3.39; N, 2.84. FT-IR (KBr) ν_{max}: 3426 (b), 1609, 1504, 1234 cm^{-1}. FAB-MS m/z = 1448.36 ($M^+ - 2C_2H_5OH$), 1018.12 (M^+ − **L1** − $2C_2H_5OH$), 587.86 ($M^+ - 2$**L1** − $2C_2H_5OH$) (Fig. S6 in ESI†).

Eu(**L2**)$_3$(C_2H_5OH)$_2$ (**3**). Elemental analysis (%): calcd for $C_{76}H_{57}F_{15}N_3O_{11}Eu$ (1625.22): C, 56.17; H, 3.54; N, 2.59. Found: C, 56.28; H, 3.59; N, 2.63. FT-IR (KBr) ν_{max}: 3440 (b), 3060, 2956, 1607, 1514, 1233 cm^{-1}. FAB-MS m/z = 1533.37 ($M^+ - 2C_2H_5OH$), 1073.18 (M^+ − **L2** − $2C_2H_5OH$), 613.14 ($M^+ - 2$**L2** − $2C_2H_5OH$) (Fig. S4 in ESI†).

Gd(**L2**)$_3$(C_2H_5OH)$_2$ (**6**). Elemental analysis (%): calcd for $C_{76}H_{57}F_{15}N_3O_{11}Gd$ (1630.51): C, 55.98; H, 3.52; N, 2.58. Found: C, 56.12; H, 3.62; N, 2.62. FT-IR (KBr) ν_{max}: 3440 (b), 3063, 2925, 1607, 1514, 1233 cm^{-1}. FAB-MS m/z = 1538.56 ($M^+ - 2C_2H_5OH$), 1078.12 (M^+ − **L2** − $2C_2H_5OH$), 618.08 ($M^+ - 2$**L2** − $2C_2H_5OH$) (Fig. S7 in ESI†).

Synthesis of Eu^{3+} complexes 2 and 4

Complexes **2** and **4** were prepared by stirring equimolar quantities of the corresponding solvated Eu^{3+} complexes and the phosphine oxide DDXPO in $CHCl_3$ solution for 24 h at room temperature (Scheme 3). The products were isolated by solvent evaporation and purified by recrystallization from a chloroform–hexane mixture (20 : 80).

Eu(**L1**)$_3$(DDXPO) (**2**). Elemental analysis (%): calcd for $C_{108}H_{71}F_{15}N_3O_9P_2Eu$ (2053.62): C, 63.16; H, 3.48; N, 2.05. Found: C, 63.24; H, 3.53; N, 2.10. FT-IR (KBr) ν_{max}: 3060, 2970, 1617, 1516, 1502, 1214, 1151 cm^{-1}. FAB-MS m/z = 1623.28 (M^+ − **L1**), 1193.20 ($M^+ - 2$**L1**), 763.11 ($M^+ - 3$**L1**) (Fig. S3 in ESI†). ^{31}P NMR (202.44 MHz, $CDCl_3$): δ (ppm) −91.92.

Eu(**L2**)$_3$(DDXPO) (4). Elemental analysis (%): calcd for $C_{111}H_{77}F_{15}N_3O_{12}P_2Eu$ (2143.40): C, 62.19; H, 3.62; N, 1.96. Found: C, 62.34; H, 3.59; N, 2.03. FT-IR (KBr) ν_{max}: 3070, 1616, 1504, 1234, 1150 cm^{-1}. FAB-MS m/z = 1683.36 (M^+ − **L2**), 1222.14 ($M^+ - 2$**L2**), 763.11 ($M^+ - 3$**L2**) (Fig. S5 in ESI†). ^{31}P NMR (202.44 MHz, $CDCl_3$): δ (ppm) −96.96 (Fig. S8 in ESI†).

Geometry optimization by Sparkle/PM3 model

Using Sparkle/PM3 model implemented in MOPAC2009 program,[58] the ground state geometries of complexes **1–6** and **A** were optimized. The high accuracy of Sparkle models in predicting the ground state geometries of lanthanide complexes has been demonstrated in previous publications.[59] The keywords used were, PM3; SPARKLE; PRECISE; BFGS; GNORM = 0.25; SCFCRT = 1D-10 (to increase the SCF convergence criterion) and *XYZ* (for Cartesian coordinates).

Experimental Judd–Ofelt parameters

The intensity parameters Ω_λ for the complexes **1–4** were determined from their emission spectra using eqn (1).

$$\Omega_\lambda = (2\lambda + 1) \sum_{t}^{\lambda-1,\lambda+1(\text{odd})} \sum_{p=-t}^{t(\text{all})} \frac{|B_{\lambda tp}|^2}{(2t+1)} \quad (1)$$

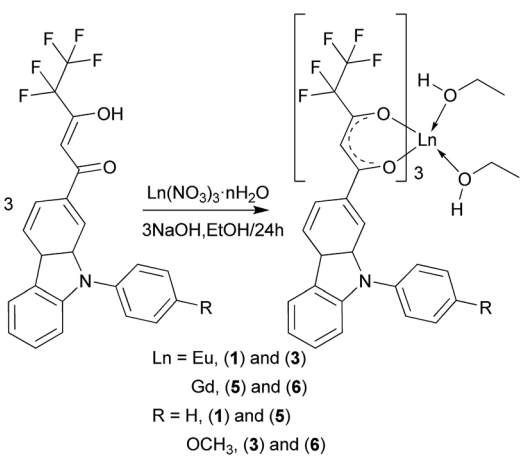

Scheme 2 Synthesis of solvated lanthanide complexes **1**, **3**, **5** and **6**.

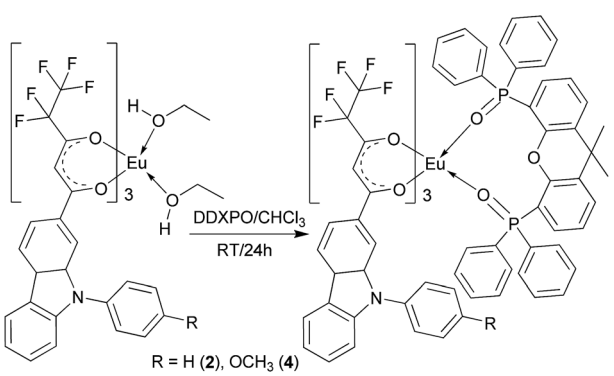

Scheme 3 Synthesis of Eu^{3+} complexes **2** and **4**.

The $B_{\lambda tp}$ are calculated by:

$$B_{\lambda tp} = B^{ed}_{\lambda tp} + B^{dc}_{\lambda tp} \quad (2)$$

To know which values each parameters (λ, t and p) assume in relation to each other is a very important aspect to facilitate the application of Judd–Ofelt theory. As indicated in eqn (1) and (2), for example, when λ is 2, t will be equal to 1 and 3, whereas the values of p will be equal to 0, 1, …, t.

The first term in eqn (2), $B^{ed}_{\lambda tp}$, refers to the forced electric-dipole (ed) contribution, which is given by eqn (3).

$$B^{ed}_{\lambda tp} = \frac{2}{\Delta E}\langle r^{t+1}\rangle\theta(t,\lambda)\gamma_p{}^t \quad (3)$$

And the second term, $B^{dc}_{\lambda tp}$, refers to the dynamic coupling (dc) contribution, given by eqn (4).

$$B^{dc}_{\lambda tp} = -\left[\frac{(\lambda+1)(2\lambda+3)}{2\lambda+1}\right]^{1/2}\langle r^{\lambda}\rangle(1-\sigma_\lambda)\langle f\|C^{(\lambda)}\|f\rangle\Gamma_p{}^t\delta_{t,\lambda+1} \quad (4)$$

where, ΔE corresponds to the energy level difference between the ground state barycenters and the first excited state configuration of the opposite parity. The radial integrals, $\langle r^{\lambda}\rangle$ were taken from reference,[60] by extrapolating the quantity $\langle r^{8}\rangle$. The terms $\theta(t,p)$ are numeric factors associated with each Ln^{3+} ion and are estimated from radial integrals of Hartree–Fock calculations.[61] $(1-\sigma_\lambda)$ is the shielding field due to 5s and 5p filled orbitals of Ln^{3+} ions, which have radial extensions larger than those of 4f orbitals. $\langle f\|C^{(\lambda)}\|f\rangle$ is a tensor operator of rank (λ = 2, 4, and 6) with values $\langle 3\|C^{(2)}\|3\rangle = -1.366$, $\langle 3\|C^{(4)}\|3\rangle = 1.128e$ $\langle 3\|C^{(6)}\|3\rangle = -1.270$ for Ln^{3+} ions. $\delta_{t,\lambda+1}$ is the Kronecker delta function. $B^{dc}_{\lambda tp}$ as such is equal to zero when t is different from $\lambda + 1$.

Results and discussion

Synthesis and characterization of ligands and Ln^{3+} complexes

The β-diketonate ligands, **L1** and **L2**, were synthesized with an overall yield of 72% and 70%, respectively using the procedure outlined in Scheme 1. The synthesized ligands were well characterized by ^{1}H NMR, ^{13}C NMR, FT-IR and mass spectroscopic (FAB-MS) methods as well as by elemental analyses. The ^{1}H NMR analyses (Fig. S1 in ESI†) reveal that the β-diketonate ligands **L1** and **L2** exist as enolic forms in chloroform solution. The synthesis procedures for the lanthanide complexes **1–6**, are illustrated in Schemes 2 and 3. The synthesized complexes were characterized by FT-IR, mass spectroscopy (FAB-MS), ^{31}P NMR and elemental analyses. The FT-IR spectra of complexes **1**, **3**, **5** and **6** exhibit a broad absorption band in the 3000–3500 cm^{-1} region, which points to the presence of coordinated solvent molecules, while the absence of this band in complexes **2** and **4** implies that the solvent molecules are replaced by the bidentate phosphine oxide ligand. The carbonyl stretching frequencies for the β-diketonate ligands, **L1** (1597 cm^{-1}) and **L2** (1595 cm^{-1}) were shifted to higher wavenumbers in the complexes (1607 cm^{-1} in **1**; 1617 cm^{-1} in **2**; 1607 cm^{-1} in **3**; 1616 cm^{-1} in **4**; 1609 cm^{-1} in **5** and 1607 cm^{-1} in **6**), indicating the coordination of carbonyl oxygen to the Ln^{3+} cation in each case. The P=O stretching frequency of free DDXPO (1190 cm^{-1}) has been shifted to lower wave numbers in complex **2** (1151 cm^{-1}) and complex **4** (1150 cm^{-1}) which confirms the involvement of phosphoryl oxygen in the complex formation. The elemental analyses and FAB-MS data (Fig. S2–S7 in ESI†) for the complexes **1–6** suggest that the central Ln^{3+} ion is coordinated to β-diketonate ligands in a metal-to-ligand mole ratio of 1 : 3. In addition to this, complexes **1**, **3**, **5** and **6** have two ethanol molecules coordinated to the metal centre satisfying the high co-ordination number of the Ln^{3+} ion. As expected in complexes **2** and **4** one molecule of the bidentate phosphine oxide, DDXPO replaces the solvent molecules from the coordination sphere of **1** and **3**, respectively. The presence of DDXPO in the coordination sphere of complexes **2** and **4** was further confirmed by the upfield shift in the ^{31}P NMR signal of complexes **2** (−91.92 ppm) and **4** (−96.96 ppm) (Fig. S8 in ESI†) compared to the free DDXPO (30.97 ppm).

Thermal behaviour of the complexes

In order to explore the thermal behaviour of the Eu^{3+} complexes, thermogravimetric analyses (TGA) of all the complexes were carried out under nitrogen atmosphere. The weight loss profiles for representative complexes **3**, **4** and **6** are displayed in Fig. 2 and that of complexes **1**, **2** and **5** are given in Fig. S9 (in ESI†). The thermogravimetric profiles of solvated complexes (**1**, **3**, **5** and **6**) exhibit a weight loss of approximately 5% in the first step (120 to 160 °C), which corresponds to the elimination of the coordinated ethanol solvent molecules (calculated as 5.99, 5.97, 5.66, 5.64% for **1**, **3**, **5** and **6**, respectively). Notably, complexes **2** and **4** are stable up to 325 °C, compared to our reference complex **A** (stable only up to 180 °C). The high thermal stability of complexes **2** and **4** further confirms the successful replacement of the coordinated ethanol molecules with the bidentate phosphine oxide molecule which in turn provides increased rigidity to the complexes.

Molecular structures of the complexes by Sparkle/PM3 model

Numerous attempts to grow single crystals for the complexes **1–6** from $CHCl_3$/ethanol and $CHCl_3$/2-methoxy ethanol solutions

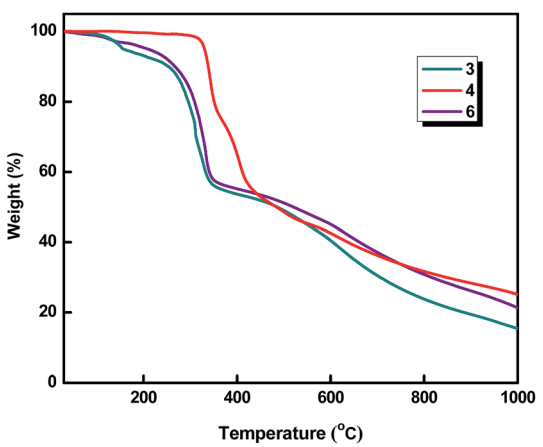

Fig. 2 Thermogravimetric curves for complexes **3**, **4** and **6**.

were not fruitful. Hence, in the present study the molecular structures of the designed complexes were determined using the Sparkle/PM3 model.[62] At the outset, we verified the suitability of this model by calculating the ground state geometry of our previously reported reference complex **A** (Fig. 1) whose crystal structure is known.[48] The geometry and spherical coordinates obtained from this calculation are compared to the reported crystal structure data (Fig. S10 and Table S1 in ESI†) and found to be in good agreement. The optimized geometries of the typical complexes **3** and **4** are depicted in Fig. 3 and 4 and that of complexes **1**, **2**, **5** and **6** are displayed in Fig. S11–S14 (in ESI†). The calculated spherical atomic coordinates of the complexes **1–6** are summarized in Tables S2–S5 in ESI.† In the solvated complexes **1**, **3**, **5** and **6** the central Ln^{3+} ions are coordinated to three β-diketonate ligands and two ethanol molecules. On the other hand, in complexes **2** and **4**, in addition to the three β-diketonate ligands, one bidentate phosphine oxide molecule is present, which replaces the two solvent molecules in the co-ordination sphere of the Eu^{3+} ions. The oxygen atom connecting the two phosphine oxide units is not involved in the coordination and consequently, the coordination number of Eu^{3+} ions in these complexes is 8. The average bond length between Eu^{3+} ion and the β-diketonate oxygen atoms in typical complex **4** is 2.469 Å, which is longer than that of Eu^{3+} and phosphoryl oxygen atoms (2.421 Å) of DDXPO. These trends are also in good accord with the crystal data reported for the complex **A**. The dihedral angle of the *N*-phenyl group to the carbazole ring is crucial for the extended π-conjugation by the phenyl group or *para*-methoxy phenyl group. These dihedral angles in complexes **1** and **2** are 45° and 31° and that in complexes **3** and **4** are 54° and 35°, respectively.

UV-visible absorption spectra

In Fig. 5 and S15 (in ESI†) the UV-visible absorption spectra of the free ligands and their corresponding Ln^{3+} complexes (in $CHCl_3$ solution, $c = 2 \times 10^{-6}$ mol L^{-1}) are depicted. The ligands **L1** and **L2** display two distinct broad bands: the band in the 315–440 nm (λ_{max} = 370 nm) region corresponds to a π–π* enolic transition of the β-diketonate moiety[48] and band in the 240–270 nm region is attributable to the π–π* transition of the

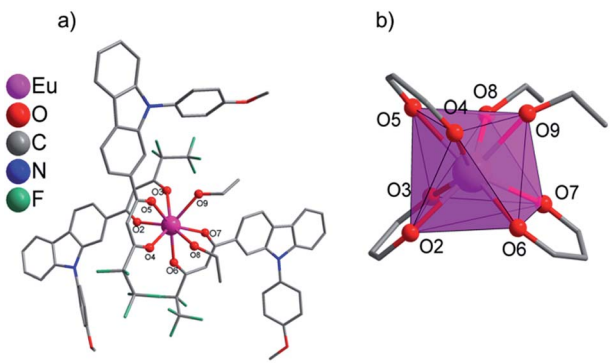

Fig. 3 (a) The ground state geometry of the complex **3** optimized by the Sparkle/PM3 model. (b) Coordination environment of complex **3**. All hydrogen atoms are omitted for clarity.

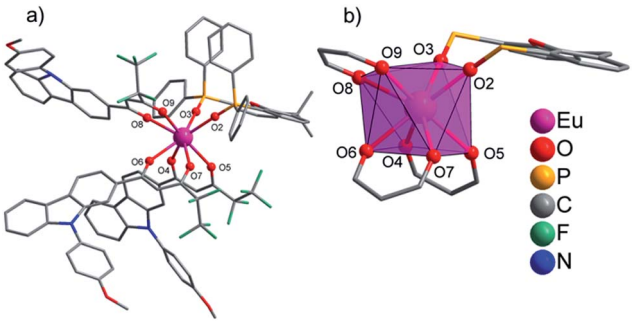

Fig. 4 (a) The ground state geometry of the complex **4** optimized by the Sparkle/PM3 model. (b) Coordination environment of complex **4**. All hydrogen atoms are omitted for clarity.

locally excited states of the carbazole backbone.[47] The large molar absorption coefficients of **L1** (3.32×10^4 L mol^{-1} cm^{-1}) and **L2** (3.41×10^4 L mol^{-1} cm^{-1}) indicate that they have a strong ability to absorb light, which is a major criteria for an organic ligand to act as a good antenna molecule.[63] Apart from a small blue shift observed due to the perturbation induced by metal coordination, the absorption spectra of the lanthanide complexes are similar to that of free ligands, indicating that the singlet excited states of the ligands are not significantly affected by the complexation to the Ln^{3+} ion. This slight blue shift indicates that the electron density on the acceptor moiety (diketonate-C_2F_5) of the ligand has been perturbed by the negative charge developed at the carbonyl oxygens which resulted from deprotonation of the ligand and the presence of Ln(III) ions with Lewis acid character.[64] The band corresponding to the electronic transitions of the chelating phosphine oxide DDXPO is also observed in the absorption spectra of complexes **2** and **4** at around 280 nm. The presence of the ancillary DDXPO ligand not only satisfies the high coordination number of the central Eu^{3+} ion but also improves the absorbance of the complexes. The molar absorption coefficient values for the complexes **1–4** were calculated at the respective λ_{max} value and found to be 8.65×10^4, 9.85×10^4, 9.05×10^4 and 9.92×10^4 L

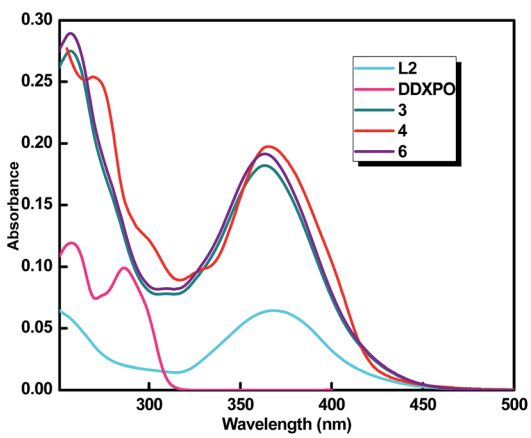

Fig. 5 UV-vis absorption spectra of the ligands **L2** and DDXPO and complexes **3**, **4** and **6** in $CHCl_3$ solution ($c = 2 \times 10^{-6}$ mol L^{-1}).

mol^{-1} cm^{-1}, respectively. The magnitudes of these absorbance values are approximately three times higher than that of the β-diketonate ligands, and this trend is compatible with the presence of three β-diketonate ligands in each complex.

Solid state absorption spectra of the complexes

To find out the effect of increased conjugation of organic ligands on the absorption spectra of the complexes, we have recorded the solid state absorption spectra of complexes **2** and **4** and compared them with that of reference complex **A** (Fig. 6). It is clear from the normalized spectra that the absorption maxima of the complexes **2** and **4** have been extended towards the visible region (410 and 420 nm, respectively) when compared to complex **A** (390 nm). By replacing the hydrogen atom of the carbazole nitrogen atom with a phenyl group we have successfully extended the π-conjugation of the molecule, which in turn shifts the absorption maximum of complex **1** towards visible region (from 390 to 410 nm). Moreover the introduction of an electron donating methoxy group on the phenyl moiety further red shifts the absorption window towards 420 nm.

Steady state photoluminescence studies

The room temperature solid state excitation and emission spectra of complexes **1–4** are given in Fig. S16 (in ESI†). The excitation spectra of the complexes **1–4** were recorded by monitoring the intense $^5D_0 \rightarrow {}^7F_2$ transition of the Eu^{3+} ion at 612 nm. Even though some sharp excitation bands due to the metal absorptions are present, the excitation spectra mainly exhibit a broad band between 250 and 500 nm region, which corresponds to the π–π* transition of the antenna ligands. Compared to the ligand absorption bands, the metal absorption peaks are weaker, which indicates that the sensitization *via* ligand excited states is more efficient than the direct excitation of the Eu^{3+} absorption bands. The normalized excitation and emission spectra of the complexes **A**, **2** and **4** are depicted in Fig. 7. The replacement of the hydrogen on the carbazole nitrogen with a phenyl ring in **L1** has increased the π-conjugation in the molecule, which remarkably extends the excitation window of complexes **1** and **2** to the visible region (λ_{max} up to 410 nm). Moreover the introduction of an electron donating $-OCH_3$ group in **L2** increases the electron density in the molecule which further red shifts the excitation window of the corresponding Eu^{3+}-complexes (complexes **3** and **4**) more towards the visible region (λ_{max} up to 420 nm). The room temperature emission spectra of Eu^{3+} complexes **1–4** exhibit the characteristically intense transitions of the Eu^{3+} ion upon excitation at 400 nm.[65] As shown in Fig. 7 and S16 (in ESI†), the radiative transitions from the excited $^5D_0$ state to the different *J* levels of the lower ^7F state were observed in the emission spectrum. Maximum peak intensities at 580, 592, 612, 652, and 702 nm were recorded for the $J = 0$, 1, 2, 3 and 4 transitions respectively.[66] The most intense transition is observed at 612 nm, corresponding to the hypersensitive $^5D_0 \rightarrow {}^7F_2$ transition and indicates that the coordination sphere of the Eu^{3+} ion is devoid of a center of symmetry. Moreover, the existence of a single chemical environment around the Eu^{3+} ion is evident from the single sharp peak corresponding to the $^5D_0 \rightarrow {}^7F_0$ transition at 580 nm.[66] The absence of broad ligand emission bands (450–530 nm) in the emission spectra of all the complexes indicates the effective sensitization of the Eu^{3+} ion by the coordinated β-diketonate ligands. From the solid state luminescence studies of complexes **1–4** (Fig. S16 in ESI†) it is clear that the displacement of the solvent molecules from the coordination spheres of the complexes $Eu(\mathbf{L1})_3(C_2H_5OH)_2$ (**1**) and $Eu(\mathbf{L2})_3(C_2H_5OH)_2$ (**3**) by the chelating phosphine oxide DDXPO in **2** and **4** significantly improves the luminescence intensity.

Luminescence decay profiles

The luminescence decay times (τ) for complexes **1–4** were recorded at room temperature at an excitation wavelength of 400 nm and monitored at the most intense emission line at 612 nm and are depicted in Fig. 8 and S17 (in ESI†). The lifetime profiles for all the Eu^{3+} complexes are fitted with single exponentials, which indicates the existence of a single chemical environment around the central Eu^{3+} ion in each case. The

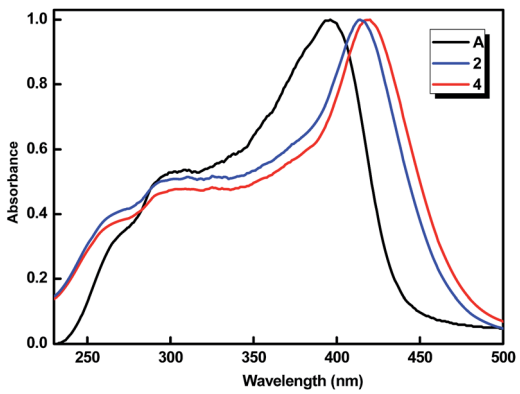

Fig. 6 Normalized solid state UV-vis absorption spectra of complexes A, 2 and 4.

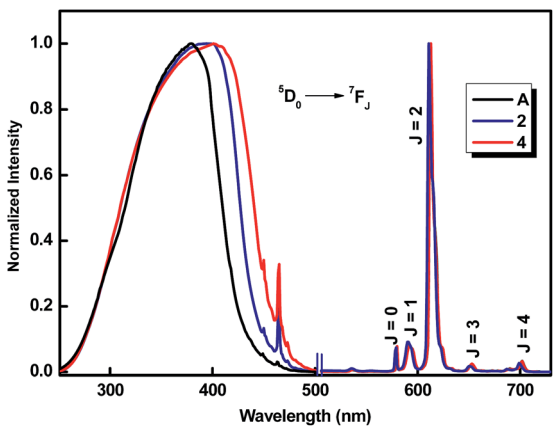

Fig. 7 Normalized solid state room-temperature excitation ($\lambda_{em} = 612$ nm) and emission ($\lambda_{ex} = 400$ nm) spectra of complexes A, 2 and 4.

relatively shorter lifetimes observed for the solvated complexes **1** and **3** may be due to the presence of high frequency oscillators in the solvent molecules, which activate the non-radiative decay pathways. In the case of the Eu^{3+} ion, the energy gap between the first excited state and the ground state levels is approximately 12 000 cm^{-1}. So, in the presence of solvent molecules, the coupling of Eu^{3+} excited states and the third vibrational overtone of the proximate OH oscillators ($\nu_{OH} \sim$ 3300–3500 cm^{-1}) will be effective, which is responsible for the quenching of luminescence in the solvated complexes **1** and **3**. On the other hand, these non-radiative decay pathways are limited in the complexes **2** and **4**, which thereby exhibit longer life time values.

By analysing the emission spectra in terms of eqn (5), the luminescence efficiencies and the relation between structure and photophysical properties of Eu^{3+} complexes can be understood in a better way.

$$Q_L^{Eu} = \eta_{sens} \times Q_{Eu}^{Eu} = \eta_{sens} \times (\tau_{obs}/\tau_{rad}) \quad (5)$$

where, η_{sens} is the efficiency of the ligand-to-metal energy transfer, Q_L^{Eu} and Q_{Eu}^{Eu} represent the overall and intrinsic luminescence quantum yields of Eu^{3+}, respectively, τ_{obs} and τ_{rad} are the observed and radiative lifetimes of Eu ($^5D_0$).[67]

Because of the low absorption intensities of direct f–f excitation, the intrinsic quantum yields of Eu^{3+} could not be determined experimentally. Therefore, the radiative lifetime of Eu^{3+} ($^5D_0$) has been calculated from eqn (6),[68]

$$1/\tau_{rad} = A_{MD,0} \times n^3 \times (I_{tot}/I_{MD}) \quad (6)$$

where, n is the refractive index (1.5), $A_{MD,0}$ represents the spontaneous emission probability for the $^5D_0 \rightarrow {}^7F_1$ transition in vacuum (14.65 s^{-1}), and I_{tot}/I_{MD} implies the ratio of the total integrated intensity of the corrected Eu^{3+} emission spectrum to the integrated intensity of the magnetic dipole $^5D_0 \rightarrow {}^7F_1$ transition. The intrinsic quantum yields for Eu^{3+} complexes have been calculated from the ratio (τ_{obs}/τ_{rad}) and the values are tabulated in Table 1. The overall quantum yields (Q_L^{Eu}), radiative (A_{RAD}) and nonradiative (A_{NR}) decay rates and energy transfer efficiencies (η_{sens}) are also listed in Table 1.

The replacement of solvent molecules by the chelating phosphine oxide molecule results in an approximately 3-fold increase in the overall quantum yield of Eu^{3+}–tris-β-diketonate complexes (from 12 to 34% in complex **2** and 15–42% in complex **4**) in the solid state. This significant increase in the overall quantum yields may be due to (i) the removal of quenching effect of the O–H vibrations, which results in the increase of intrinsic quantum yields from 28% (in **1**) and 32% (in **3**) to 64% (in **2**) and 63% (in **4**) and (ii) the enhancement of η_{sens} from 43% (in **1**) to 52% (in **2**) and 47% (in **3**) to 66% (in **4**).

Determination of the relevant electronic states of the ligands is important to investigate the photoluminescence mechanism of the Eu^{3+} complexes. The singlet (S1) energy levels of the ligands **L1** and **L2** were estimated by referring to the upper wavelengths of the UV-vis absorption edges of Gd(**L1**)$_3$(C_2H_5OH)$_2$ and Gd(**L2**)$_3$(C_2H_5OH)$_2$ complexes, respectively. The triplet (T1) energy levels of the ligands were calculated by referring to the lower wavelength emission edges of the corresponding phosphorescence spectra of complexes Gd(**L1**)$_3$(C_2H_5OH)$_2$ (**5**) and Gd(**L2**)$_3$(C_2H_5OH)$_2$ (**6**) (Fig. S18 in ESI†). Thus, the S1 and T1 values for **L1** were found to be 24 190 cm^{-1} and 20 660 cm^{-1}, respectively. The S1 and T1 values for **L2** were found to be 24 100 cm^{-1} and 20 550 cm^{-1} respectively. The S1 (31 850 cm^{-1}) and T1 (23 470 cm^{-1}) levels for the ancillary ligand DDXPO were taken from our earlier report.[50] The triplet energy levels of the ligands **L1** and **L2** are found to have significantly higher energy than that of the $^5D_0$ state of Eu^{3+}, proving that the novel β-diketonate ligands can act as antenna molecules for the photosensitization of the Eu^{3+} ion.[69] However, the higher $^5D_1$ emitting state of Eu^{3+} (18 800 cm^{-1}) appears critically close to the triplet states of the **L1** and **L2** ligands, which can bring about the thermally assisted back-energy transfer from the Eu^{3+} ion.[70] On the other hand, the triplet energy level of the bidentate DDXPO (23 470 cm^{-1}), is suitable for efficient energy transfer with all the $^5D_2$, $^5D_1$ and $^5D_0$ energy levels of Eu^{3+} ion. Therefore, the photoluminescence mechanism in the Eu^{3+} complexes is proposed to be a ligand sensitized luminescence process, the antenna effect. Based on the preceding observations, the schematic representation of energy level diagrams showing the possible energy transfer mechanism for complex **4** is depicted in Fig. 9.

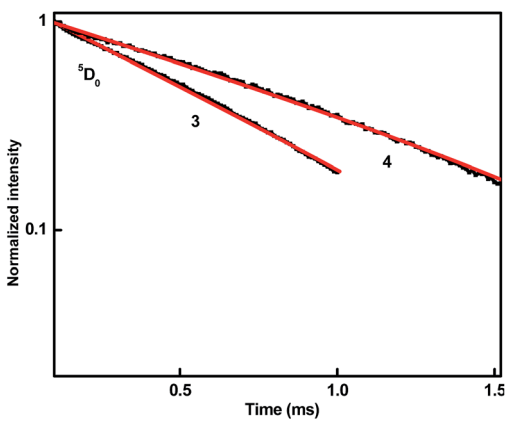

Fig. 8 Solid state luminescence decay profiles of complexes **3** and **4** monitored at 612 nm.

Table 1 Radiative (A_{RAD}) and non-radiative (A_{NR}) decay rates, $^5D_0$ lifetime (τ_{obs}), intrinsic quantum yield (Q_{Eu}^{Eu}, %), energy transfer efficiency (η_{sens}, %) and overall quantum yield (Q_L^{Eu}, %) for complexes **1–4**

Compound	A_{RAD}/s^{-1}	A_{NR}/s^{-1}	$\tau_{obs}/\mu s$	Q_{Eu}^{Eu}, (%)	η_{sens}, (%)	Q_L^{Eu}, (%)
1	623	1994	382 ± 1	28	43	12
2	755	433	842 ± 1	64	52	34
3	793	1924	368 ± 1	32	47	15
4	757	451	828 ± 1	63	66	42

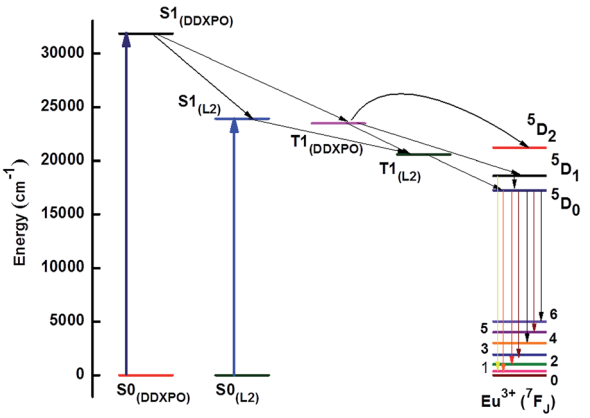

Fig. 9 Schematic representation of the energy transfer mechanism for complex **4**.

Comparison of experimental and theoretical luminescent parameters

The LUMPAC software, developed by Freire and coworkers,[49] was used to calculate the theoretical luminescent values of intensity parameters (Ω_λ), radiative emission rate (A_{RAD}), non-radiative emission rate (A_{NR}), intrinsic quantum yield (Q_{Eu}^{Eu}), and overall quantum yield (Q_L^{Eu}).

The experimental intensity parameters of the complexes **1–4** were calculated from the emission spectra, based on the Judd–Ofelt theory which provides a simple model for reproducing the intensities of f–f transitions within the frame of the crystal-field concept.[71,72] The theory assumes that the central metal ion is affected by the nearest neighbour atoms, through a static electric field which is also known as crystal or ligand field. The intensity parameters, Ω_2 and Ω_4 were experimentally calculated from the $^5D_0 \rightarrow {}^7F_2$ and $^5D_0 \rightarrow {}^7F_4$ electronic transitions of the corresponding Eu^{3+} ions and describe the interaction between the lanthanide ion and the ligands. The experimental and theoretical values for the intensity parameters (Ω_2, Ω_4 and Ω_6) are depicted in Table 2, and are in excellent agreement with each other. The experimental Ω_6 value could not be calculated due to the absence of $^5D_0 \rightarrow {}^7F_6$ transition in the emission spectra and hence the intensity parameter Ω_6 can be determined only theoretically. The high values obtained for Ω_2 may be due to the hypersensitive nature of the $^5D_0 \rightarrow {}^7F_2$ transition and implies that the dynamic coupling mechanism is operative. This also indicates the presence of a highly polarisable chemical environment in the Eu^{3+} complexes. Compared to Ω_2, Ω_4 is less sensitive to the coordination environment and the relatively low values of Ω_4 point to the rigidity associated with the coordination sphere of the synthesized Eu^{3+} complexes. The theoretical calculations were carried out as described in our recent report.[73] The experimental and theoretical values of the radiative (A_{RAD}) and non-radiative (A_{NR}) decay rates, intrinsic quantum yields (Q_{Eu}^{Eu}, %) and overall quantum yields (Q_L^{Eu}, %) are also summarized in Table 2.

Table 2 Experimental and theoretical intensity parameters Ω_2, Ω_4 and Ω_6, radiative (A_{RAD}) and non-radiative (A_{NR}) decay rates, intrinsic quantum yield (Q_{Eu}^{Eu}, %) and overall quantum yield (Q_L^{Eu}, %) values derived from the optimized Sparkle/PM3 structure[a]

Compound	Ω_2	Ω_4	Ω_6	A_{RAD}/s^{-1}	A_{NR}/s^{-1}	Q_{Eu}^{Eu}, (%)	Q_L^{Eu}, (%)
1a	17.60	3.09	—	623	1994	28	12
1b	17.59	3.09	0.12	627	1990	24	10
2a	21.60	2.51	—	755	433	64	34
2b	21.57	2.37	0.24	737	451	62	24
3a	23.51	2.71	—	793	1924	32	15
3b	23.51	2.70	0.36	800	1917	30	18
4a	21.10	2.59	—	757	451	63	42
4b	21.11	2.39	0.045	723	485	60	57

[a] The values of the intensity parameters are presented in 10^{-20} cm^2. a = experimental, b = theoretical.

The intrinsic quantum yield values of the complexes obtained experimentally and theoretically are perfectly matching. In the case of overall quantum yield, even though the experimentally and theoretically calculated values follow the same trend in general, there is a slight variation in the exact figures. This may be due to considerable dependence of the theoretically calculated quantum yield values on the triplet energies of the complexes.

Conclusions

In this work, we have reported the synthesis, characterization and photophysical properties of a series of carbazole-based fluorinated β-diketonate europium complexes. The novel ligands were designed by introducing a phenyl group or a *para* methoxy phenyl group on the nitrogen atom of the carbazole ring in complexes **1** and **3**, respectively. Replacement of solvent molecules in **1** and **3** by the ancillary ligand, bidentate phosphine oxide DDXPO led to complexes **2** and **4** respectively. The molecular geometries of the designed complexes were optimized by the Sparkle/PM3 model. The suitability of Sparkle/PM3 model was verified by comparing the ground state geometry of our previously reported related complex **A**, with its crystal structure. Complexes **2** and **4** showed remarkable overall quantum yields of 34% and 42% and excellent lifetime values of 842 μs and 828 μs respectively. They also exhibited impressive thermal stabilities up to 325 °C. The excitation window was extended from 390 nm into the visible region by the introduction of a phenyl ring on the carbazole ring, giving **1** and **2**, (up to 410 nm) and further by the introduction of an electron donating *para*-methoxy group onto the phenyl ring in **3** and **4** (up to 420 nm). This shift achieved from near UV to visible blue region is important in the context of biological imaging as long term exposure of near UV light may destroy the cells under study and also the surrounding cells around the target area, in case of *in vivo* experiments. The theoretical luminescent properties of the designed Eu^{3+} complexes were calculated based on the optimized Sparkle/PM3 structure using the LUMPAC software and were in good agreement with the experimental values, proving the suitability of the Sparkle/PM3 model. Thus, the dramatic improvements in the thermal stabilities, photophysical properties and excitation window, brought about by the introduction

of extended conjugation and ancillary ligand; emphasize the significance of molecular engineering of ligand and complexes to achieve desired properties.

Acknowledgements

The authors acknowledge financial support from Council of Scientific and Industrial Research, New Delhi (NWP-55). B. F. thanks CSIR and DAAD for the fellowships.

Notes and references

1 S. J. Butler, M. Delbianco, L. Lamarque, B. K. McMahon, E. R. Neil, R. Pal, D. Parker, J. W. Walton and J. M. Zwier, *Dalton Trans.*, 2015, 4791–4803.
2 M. Rajendran, E. Yapici and L. W. Miller, *Inorg. Chem.*, 2014, **53**, 1839–1853.
3 D. Geißler, S. Linden, K. Liermann, K. D. Wegner, L. J. Charbonnière and N. Hildebrandt, *Inorg. Chem.*, 2014, **53**, 1824–1838.
4 J.-C. G. Bunzli and S. V. Eliseeva, *Chem. Sci.*, 2013, **4**, 1939–1949.
5 E. G. Moore, A. P. S. Samuel and K. N. Raymond, *Acc. Chem. Res.*, 2009, **42**, 542–552.
6 D. Ananias, F. A. A. Paz, D. S. Yufit, L. D. Carlos and J. Rocha, *J. Am. Chem. Soc.*, 2015, **137**, 3051–3058.
7 S. M. Borisov, R. Fischer, R. Saf and I. Klimant, *Adv. Funct. Mater.*, 2014, **24**, 6548–6560.
8 Y. Li, S. Zhang and D. Song, *Angew. Chem., Int. Ed.*, 2013, **52**, 710–713.
9 H. Peng, M. I. J. Stich, J. Yu, L.-n. Sun, L. H. Fischer and O. S. Wolfbeis, *Adv. Mater.*, 2010, **22**, 716–719.
10 B. V. Harbuzaru, A. Corma, F. Rey, J. L. Jordá, D. Ananias, L. D. Carlos and J. Rocha, *Angew. Chem., Int. Ed.*, 2009, **48**, 6476–6479.
11 K. Ai, B. Zhang and L. Lu, *Angew. Chem., Int. Ed.*, 2009, **48**, 304–308.
12 Y. Hasegawa and T. Nakanishi, *RSC Adv.*, 2015, **5**, 338–353.
13 P. P. Lima, F. A. A. Paz, C. D. S. Brites, W. G. Quirino, C. Legnani, M. Costa e Silva, R. A. S. Ferreira, S. A. Júnior, O. L. Malta, M. Cremona and L. D. Carlos, *Org. Electron.*, 2014, **15**, 798–808.
14 J. Wu, J. Wang, J. Lin, Y. Xiao, G. Yue, M. Huang, Z. Lan, Y. Huang, L. Fan, S. Yin and T. Sato, *Sci. Rep.*, 2013, **3**, 2058–2063.
15 M. Pietraszkiewicz, M. Maciejczyk, I. D. W. Samuel and S. Zhang, *J. Mater. Chem. C*, 2013, **1**, 8028–8032.
16 J. Kido and Y. Okamoto, *Chem. Rev.*, 2002, **102**, 2357–2368.
17 S. F. H. Correia, V. de Zea Bermudez, S. J. L. Ribeiro, P. S. Andre, R. A. S. Ferreira and L. D. Carlos, *J. Mater. Chem. A*, 2014, **2**, 5580–5596.
18 A. de Bettencourt-Dias, *Dalton Trans.*, 2007, 2229–2241.
19 H. Kataoka, S. Omagari, T. Nakanishi and Y. Hasegawa, *Opt. Mater.*, 2015, **42**, 411–416.
20 S. Zou, Q. Li and S. Du, *RSC Adv.*, 2015, **5**, 34936–34941.
21 B. Francis, D. B. Ambili Raj and M. L. P. Reddy, *Dalton Trans.*, 2010, 8084–8092.
22 L. D. Carlos, R. A. S. Ferreira, V. d. Z. Bermudez and S. J. L. Ribeiro, *Adv. Mater.*, 2009, **21**, 509–534.
23 K. Binnemans, *Chem. Rev.*, 2009, **109**, 4283–4374.
24 J.-C. G. Bunzli and C. Piguet, *Chem. Soc. Rev.*, 2005, **34**, 1048–1077.
25 K. Machado, S. Mukhopadhyay, R. A. Videira, J. Mishra, S. M. Mobin and G. S. Mishra, *RSC Adv.*, 2015, **5**, 35675–35682.
26 A. J. Amoroso and S. J. A. Pope, *Chem. Soc. Rev.*, 2015, **44**, 4723–4742.
27 G. F. de Sá, O. L. Malta, C. de Mello Donegá, A. M. Simas, R. L. Longo, P. A. Santa-Cruz and E. F. da Silva Jr, *Coord. Chem. Rev.*, 2000, **196**, 165–195.
28 S. M. Bruno, D. Ananias, F. A. Almeida Paz, M. Pillinger, A. A. Valente, L. D. Carlos and I. S. Goncalves, *Dalton Trans.*, 2015, 488–492.
29 N. Sabbatini, M. Guardigli and J.-M. Lehn, *Coord. Chem. Rev.*, 1993, **123**, 201–228.
30 J.-M. Lehn, *Angew. Chem., Int. Ed.*, 1990, **29**, 1304–1319.
31 J. Feng and H. Zhang, *Chem. Soc. Rev.*, 2013, **42**, 387–410.
32 S. Biju, L. Xu, C.-Z. Sun and Z.-N. Chen, *J. Mater. Chem. C*, 2015, **3**, 5775–5782.
33 S. Raphael, M. L. P. Reddy, K. V. Vasudevan and A. H. Cowley, *Dalton Trans.*, 2012, 14671–14682.
34 P. He, H. H. Wang, S. G. Liu, J. X. Shi, G. Wang and M. L. Gong, *Inorg. Chem.*, 2009, **48**, 11382–11387.
35 S. V. Eliseeva and J.-C. G. Bunzli, *Chem. Soc. Rev.*, 2010, **39**, 189–227.
36 J.-C. G. Bünzli, *Chem. Rev.*, 2010, **110**, 2729–2755.
37 C. P. Montgomery, B. S. Murray, E. J. New, R. Pal and D. Parker, *Acc. Chem. Res.*, 2009, **42**, 925–937.
38 M. Irfanullah, D. K. Sharma, R. Chulliyil and A. Chowdhury, *Dalton Trans.*, 2015, 3082–3091.
39 V. Divya and M. L. P. Reddy, *J. Mater. Chem. C*, 2013, **1**, 160–170.
40 V. Divya, R. O. Freire and M. L. P. Reddy, *Dalton Trans.*, 2011, 3257–3268.
41 A. Dadabhoy, S. Faulkner and P. G. Sammes, *J. Chem. Soc., Perkin Trans. 2*, 2002, 348–357.
42 A. Dadabhoy, S. Faulkner and P. G. Sammes, *J. Chem. Soc., Perkin Trans. 2*, 2000, 2359–2360.
43 A. D'Aléo, A. Picot, A. Beeby, J. A. Gareth Williams, B. Le Guennic, C. Andraud and O. Maury, *Inorg. Chem.*, 2008, **47**, 10258–10268.
44 M. L. P. Reddy, V. Divya and R. Pavithran, *Dalton Trans.*, 2013, 15249–15262.
45 V. Divya, V. Sankar, K. G. Raghu and M. L. P. Reddy, *Dalton Trans.*, 2013, 12317–12323.
46 P. He, H. H. Wang, H. G. Yan, W. Hu, J. X. Shi and M. L. Gong, *Dalton Trans.*, 2010, 8919–8924.
47 P. He, H. H. Wang, S. G. Liu, J. X. Shi and M. L. Gong, *Appl. Phys. B: Lasers Opt.*, 2010, **99**, 757–762.
48 D. B. A. Raj, B. Francis, M. L. P. Reddy, R. R. Butorac, V. M. Lynch and A. H. Cowley, *Inorg. Chem.*, 2010, **49**, 9055–9063.
49 J. D. L. Dutra, T. D. Bispo and R. O. Freire, *J. Comput. Chem.*, 2014, **35**, 772–775.

50 D. B. Ambili Raj, S. Biju and M. L. P. Reddy, *Dalton Trans.*, 2009, 7519–7528.
51 L. Porrès, A. Holland, L.-O. Pålsson, A. Monkman, C. Kemp and A. Beeby, *J. Fluoresc.*, 2006, **16**, 267–273.
52 L. O. Pålsson and A. P. Monkman, *Adv. Mater.*, 2002, **14**, 757–758.
53 J. C. de Mello, H. F. Wittmann and R. H. Friend, *Adv. Mater.*, 1997, **9**, 230–232.
54 M. S. Wrighton, D. S. Ginley and D. L. Morse, *J. Phys. Chem.*, 1974, **78**, 2229–2233.
55 N. S. S. Kumar, S. Varghese, N. P. Rath and S. Das, *J. Phys. Chem. C*, 2008, **112**, 8429–8437.
56 M. Cölle, J. Gmeiner, W. Milius, H. Hillebrecht and W. Brütting, *Adv. Funct. Mater.*, 2003, **13**, 108–112.
57 S. V. Eliseeva, O. V. Kotova, F. Gumy, S. N. Semenov, V. G. Kessler, L. S. Lepnev, J.-C. G. Bünzli and N. P. Kuzmina, *J. Phys. Chem. A*, 2008, **112**, 3614–3626.
58 M. R. Felicio, T. G. Nunes, P. M. Vaz, A. M. P. Botas, P. Ribeiro-Claro, R. A. S. Ferreira, R. O. Freire, P. D. Vaz, L. D. Carlos, C. D. Nunes and M. M. Nolasco, *J. Mater. Chem. C*, 2014, **2**, 9701–9711.
59 D. A. Rodrigues, N. B. da Costa and R. O. Freire, *J. Chem. Inf. Model.*, 2011, **51**, 45–51.
60 A. J. Freeman and J. P. Desclaux, *J. Magn. Magn. Mater.*, 1979, **12**, 11–21.
61 O. L. Malta, S. J. L. Ribeiro, M. Faucher and P. Porcher, *J. Phys. Chem. Solids*, 1991, **52**, 587–593.
62 R. O. Freire, G. B. Rocha and A. M. Simas, *J. Braz. Chem. Soc.*, 2009, **20**, 1638–1645.
63 M. L. P. Reddy and S. Sivakumar, *Dalton Trans.*, 2013, 2663–2678.
64 A. W. Woodward, A. Frazer, A. R. Morales, J. Yu, A. F. Moore, A. D. Campiglia, E. V. Jucov, T. V. Timofeeva and K. D. Belfield, *Dalton Trans.*, 2014, 16626–16639.
65 L. Armelao, S. Quici, F. Barigelletti, G. Accorsi, G. Bottaro, M. Cavazzini and E. Tondello, *Coord. Chem. Rev.*, 2010, **254**, 487–505.
66 K. Binnemans, *Coord. Chem. Rev.*, 2015, **295**, 1–45.
67 N. M. Shavaleev, S. V. Eliseeva, R. Scopelliti and J.-C. G. Bünzli, *Inorg. Chem.*, 2010, **49**, 3927–3936.
68 M. H. V. Werts, R. T. F. Jukes and J. W. Verhoeven, *Phys. Chem. Chem. Phys.*, 2002, **4**, 1542–1548.
69 M. Latva, H. Takalo, V.-M. Mukkala, C. Matachescu, J. C. Rodríguez-Ubis and J. Kankare, *J. Lumin.*, 1997, **75**, 149–169.
70 N. Armaroli, G. Accorsi, F. Barigelletti, S. M. Couchman, J. S. Fleming, N. C. Harden, J. C. Jeffery, K. L. V. Mann, J. A. McCleverty, L. H. Rees, S. R. Starling and M. D. Ward, *Inorg. Chem.*, 1999, **38**, 5769–5776.
71 G. S. Ofelt, *J. Chem. Phys.*, 1962, **37**, 511–520.
72 B. R. Judd, *Phys. Rev.*, 1962, **127**, 750–761.
73 J. D. L. Dutra and R. O. Freire, *J. Photochem. Photobiol., A*, 2013, **256**, 29–35.